EVALUATION OF A HIGHLY ANTICLASTIC PANEL WITH TOW OVERLAPS

K. Chauncey Wu
NASA Langley Research Center

Zafer Gürdal
Delft University of Technology

ABSTRACT

A rectangular, variable-stiffness panel with tow overlaps was manufactured using an advanced tow placement machine. The cured panel had large anticlastic imperfections, with measured amplitudes of over two times the average panel thickness. These imperfections were not due to the overall steered-fiber layup or the tow overlaps, but instead resulted from local asymmetries in the laminate that were caused by a manufacturing oversight. In the nominal panel layup, fiber angles vary linearly from ±60 degrees on the panel axial centerline to ±30 degrees on the parallel edges.

A geometrically nonlinear analysis was performed with a –280 degree Fahrenheit thermal load to simulate the postcure cooldown to room temperature. The predicted geometric imperfections correlated well with the measured panel shape. Unique structural test fixtures were then developed which greatly reduced these imperfections, but they also caused prestresses in the panel. Surface imperfections measured after the panel was installed in the test fixtures were used with nonlinear finite element analyses to predict these fixturing-induced prestresses. These prestresses were also included in structural analyses of panel end compression to failure, and the analytical results compared well with test data when both geometric and material nonlinearities were included.

INTRODUCTION

Typically, a composite panel that is laid up and cured on a planar tool surface is intended to remain perfectly flat in service. However, it is very common for a completed structure to have one or more finite radii of curvature after curing.

K. Chauncey Wu, Aerospace Engineer, Structural Mechanics and Concepts Branch, RTD, NASA Langley Research Center. Mail Stop 190, Hampton, VA 23681

Zafer Gürdal, Aerospace Structures Chair, Faculty of Aerospace Engineering, Delft University of Technology. Kluyverweg 1, 2629 HS Delft, Delft, The Netherlands.

Depending on the laminate layup, these cured shapes can resemble a cylindrical sector, a shallow bowl, or an anticlastic surface [1,2].

The resulting structural performance of such panels can also be difficult to evaluate because of their nonplanar configuration. Previous experimental studies have employed test fixtures that have somewhat limited capabilities to remove these manufacturing-induced geometric imperfections [3,4]. The objective of this work is to illustrate the application of a mechanical system to reduce or remove anticlastic geometric imperfections from a complicated composite panel. Additionally, the effects of these fixtures on the panel are modeled using finite element structural analyses, and the level of detail required to do so is assessed.

In this study, a panel with large anticlastic imperfections was evaluated using a combination of experimental methods and nonlinear (both geometric and material) finite element analyses. The panel was studied at several key points in its lifetime. First, the measured panel shape at room temperature was compared with results from a finite element analysis of the postcure cooldown of the panel to room temperature from its cure temperature.

The panel with its resulting anticlastic imperfections was then prepared for end compression loading by attaching specially designed structural test fixtures that also serve to greatly reduce the geometric imperfections. However, this process also imposed a mechanical prestress state on the panel. These unknown internal prestresses were modeled using both finite element analyses and the measured panel imperfections recorded both with and without the structural test fixtures.

In the final step, the panel was loaded in end compression using an applied displacement, and the resulting strains and displacements were measured. A structural analysis model of the panel was used to replicate the panel response to the end shortening, and the effect of prestress and material nonlinearity was evaluated and compared with the test data.

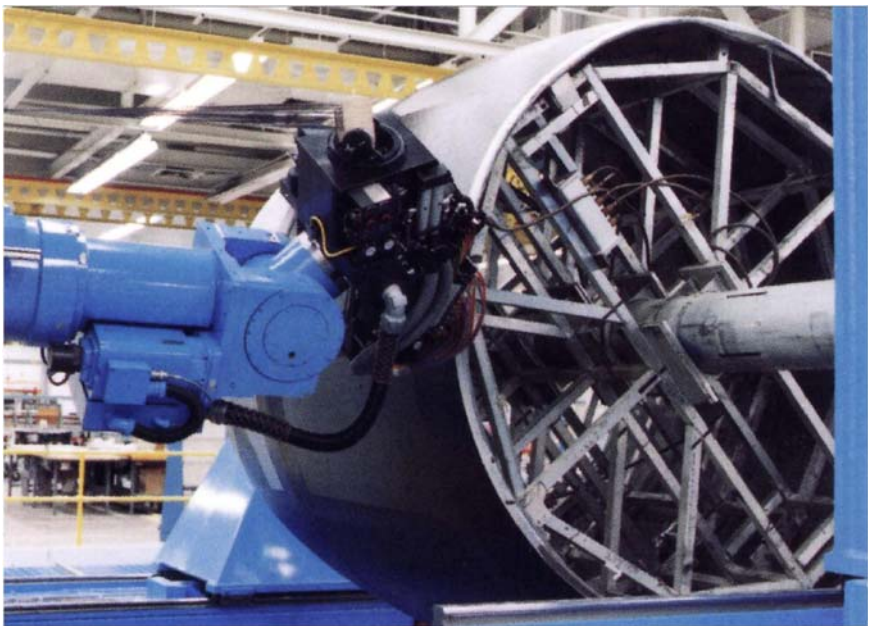

Figure 1. Fiber placement system (courtesy of Cincinnati Machine).

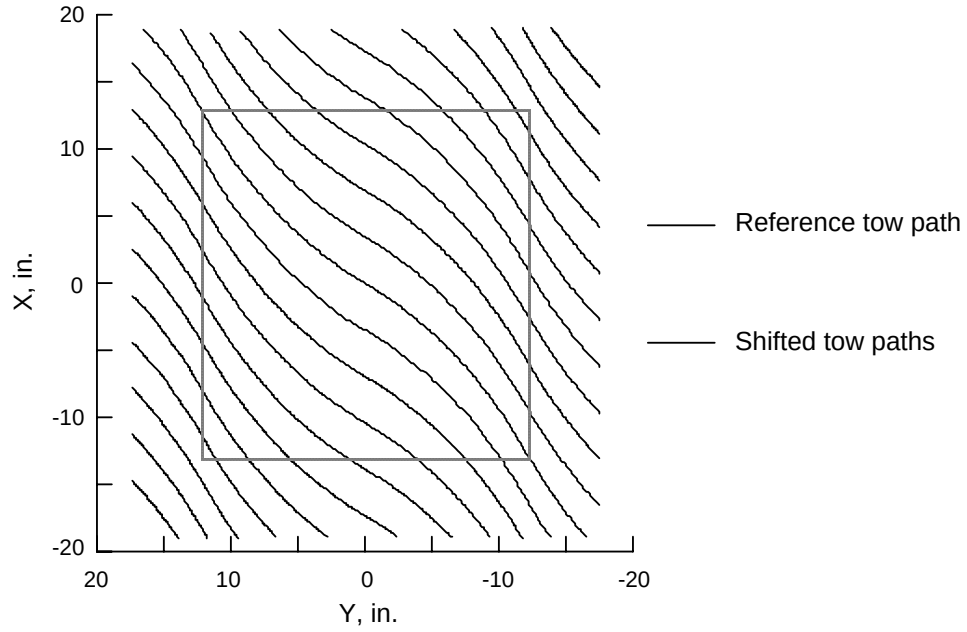

Figure 2. Variable stiffness ply tow paths.

PANEL DESIGN, MANUFACTURE AND CURE

A rectangular composite panel [5] with a 26 x 24.5-inch planform was fabricated using a commercial system [6] for computer-controlled placement of composite tows (see Figure 1). For the panel evaluated in this study, the variable stiffness layup [7] within each ply has a fiber orientation angle is allowed to vary as a function of its location on the structure's planform. Therefore, each point on the panel planform has a unique stacking sequence and number of plies.

The fiber angle (oriented with respect to the panel axial centerline) for a variable stiffness ply of this panel is illustrated in Figure 2, and decreases linearly from 60 degrees along the axial centerline, to 30 degrees near the panel edges 12 inches away. These variable stiffness plies (denoted by the Greek letter Θ) comprise the interior 16 plies of the nominal 20-ply $[\pm 45/(\pm\Theta)_4]_S$ panel layup.

The automated system used to fabricate this panel could place up to 24 tows in a single course, or pass of the fiber placement head. Courses were spaced so that neighboring tows from adjacent courses within the same ply just touch along the panel axial centerline. With each successive ply, tow overlaps were formed that increase in size towards the panel edges, as shown in Figure 3. The predicted tow overlap thicknesses in this figure were computed from the actual manufacturing input files used to fabricate the panel.

The tow-steered panel was laid up on a flat tool surface. The face of the panel in contact with the tool surface was designated as the front of the panel, while the back of the panel has the raised pattern of tow overlaps. After fabrication, the tow-steered panel was prepared and cured according to the material supplier's recommendations, and the finished panel was then cut to its final dimensions of 26 x 24.5 inches.

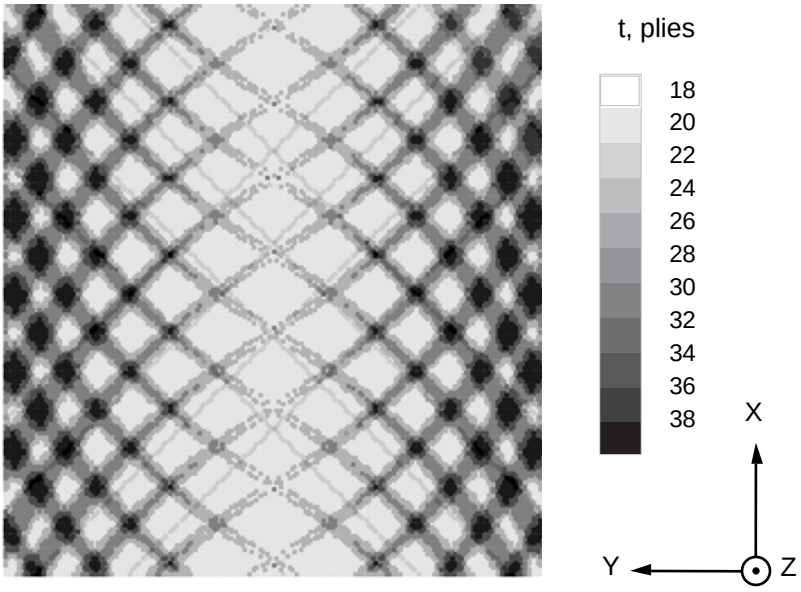

Figure 3. Predicted panel thicknesses.

CURED PANEL TEST AND ANALYSIS

The anticlastic shape of the cured panel was determined at room temperature using a high-precision coordinate measuring machine. The coordinate measuring machine was used to locate panel front and back surface spatial coordinates on a 1/8-inch square grid within the central 24-inch square test section. Note that no data were collected in the region around the test section. The difference between these front and back coordinates is the panel thickness, which is plotted in Figure 4. These measured thicknesses range from a maximum of 0.289 inches to a minimum value of 0.140 inches, with an average thickness of 0.183 inches.

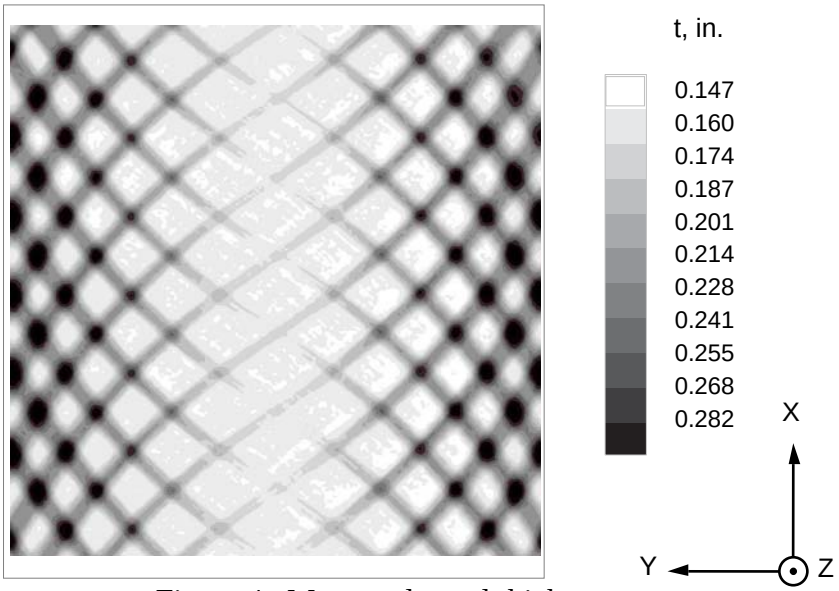

Figure 4. Measured panel thicknesses.

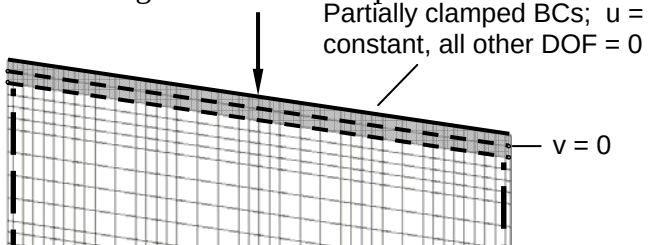

Figure 5. Panel finite element model.

A discretized structural analysis model (Figure 5) of the panel was built using the STAGS finite element code [8]. The laminate thickness, layup and midplane Z-offset at the center of each finite element were determined from the panel manufacturing data discussed above. The resulting discretized laminate thicknesses and variable stiffness ply fiber angles are shown in Figures 6 and 7, respectively.

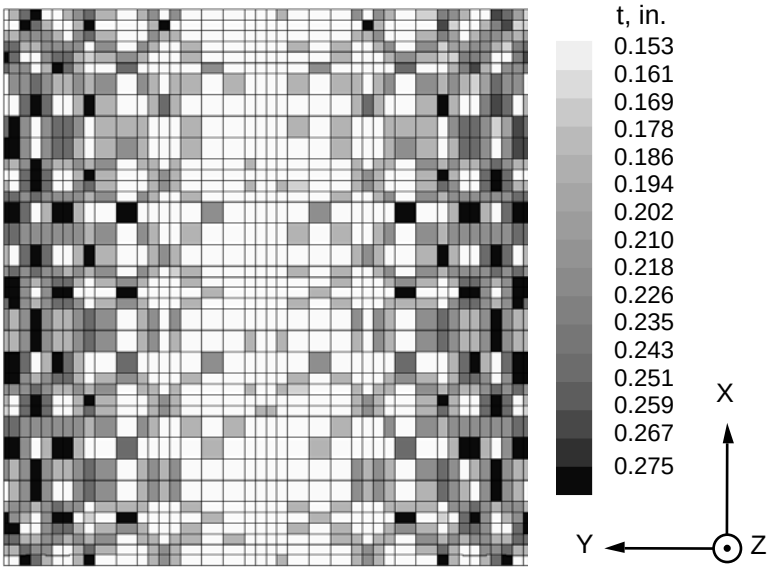

Figure 6. Panel model laminate thicknesses.

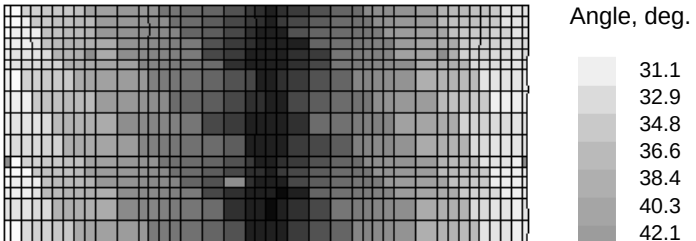

Figure 7. Panel model ply angles (ply 3 shown).

The measured panel front surface coordinates were then applied as normal displacements in a geometrically nonlinear finite element analysis of the flat panel. The predicted normal deflections surrounding the test section were then used to fill in data for the unmeasured region of the panel, and considered to be part of the measured data. The full set of imperfections for the cured panel (both measured inside the test section and the supplemental predicted deflections) is shown in Figure 8. These deflections have a maximum value of 0.450 inches, and a minimum value of –0.347 inches, which are, respectively, between 2.46 and 1.90 times the average panel thickness. The root-mean-square normal deflection of 0.176 inches is 96 percent of the average panel thickness, illustrating the magnitude of the cured panel imperfections.

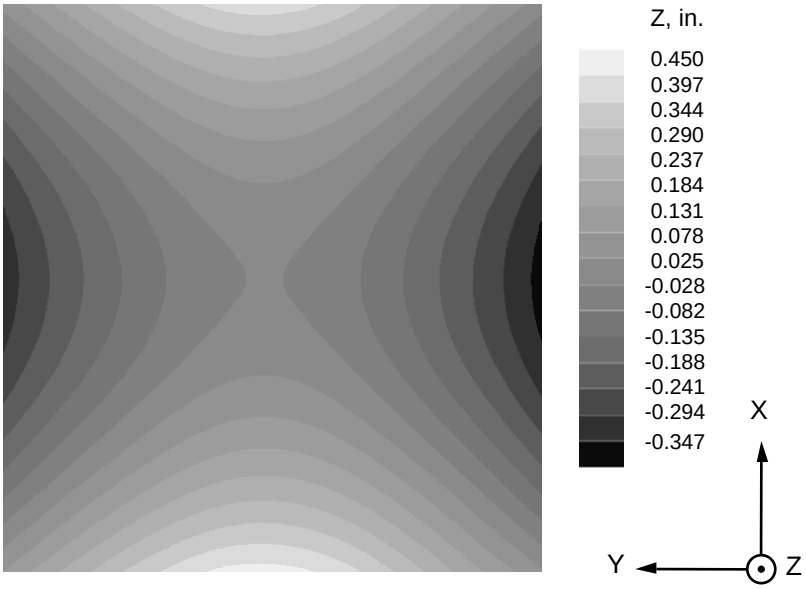

Figure 8. Measured imperfections without test fixtures.

To simulate postcure cooldown of the panel from a nominal 350 degree cure temperature to room temperature, a geometrically nonlinear finite element analysis was performed using a uniform thermal load of $\Delta T = -280$ degrees Fahrenheit

applied to the initially flat panel. Analysis boundary conditions were designed to simulate a free-free panel. The resulting predicted deflections for the cured panel are qualitatively identical to those shown in Figure 9, with a maximum value of 0.411 inches and a minimum value of –0.392 inches. These predicted extremes are within 13 percent of their corresponding measured values. The predicted root-mean-square deflection is 0.179 inches, which is within 2 percent of the measured value of 0.176 inches.

STRUCTURAL TEST FIXTURE DESIGN AND APPLICATION

The large anticlastic imperfections that resulted from the postcuring cooldown to room temperature posed a difficult problem for structural testing of the cured panel. One possible solution would have entailed constraining the loaded panel ends in epoxy potting, while leaving the vertical edges unconstrained. However, this test configuration could allow wide column buckling behavior of the panel, which would not permit realistic assessment of any buckling load variation due to the variable stiffness layup.

To address these concerns, a set of specially designed test fixtures was designed and fabricated. These test fixtures served two complementary purposes. First, they were designed to reduce or remove the large anticlastic imperfections described above. Secondly, the test fixtures were also designed to serve as the appropriate structural boundary conditions for an end-compression test of the panel. The loaded horizontal panel edges would be potted (approximating a clamped condition) and the vertical edges of the panel would be simply supported. Since all four edges of the panel would be constrained, the resulting buckling modes of the panel under end

Figure 9. Vertical edge test fixture.

Figure 10. Horizontal edge test fixture.

compression would then be forced to have at least one half-wave in both the axial and transverse directions.

In essence, both types of test fixtures developed for the horizontal and vertical panel edges function much like a common C-clamp, wherein rotation of a threaded fitting drives two clamping surfaces closer together. The test fixture design for the vertical panel edges is shown in Figure 9 and resembles a continuous C-clamp that is extruded along the panel's length. For the horizontal edge fixture shown in Figure 10, each test fixture had seven discrete pairs of threaded rods with attached swiveling pads evenly spaced along a rectangular frame (welded from steel L-channel) that encompassed the width of the panel.

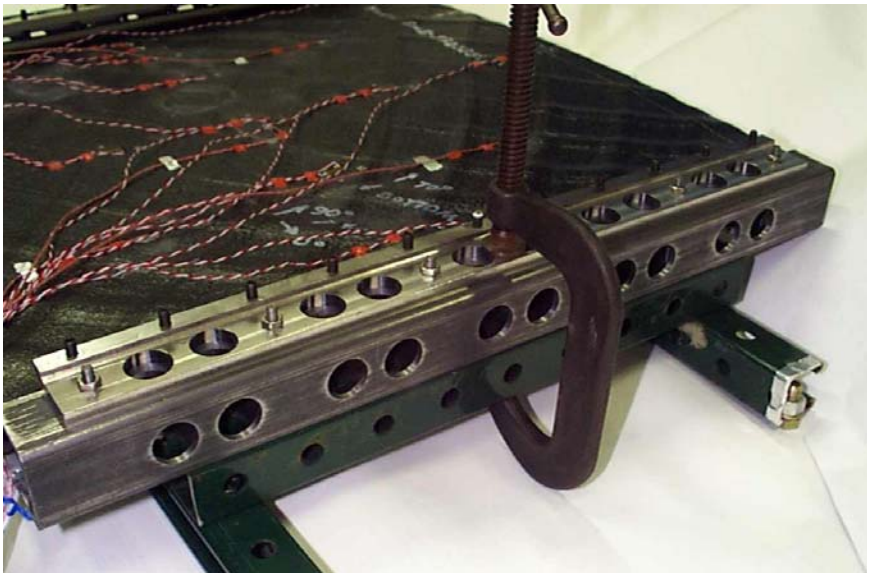

Figure 11. Panel with vertical edge fixtures installed.

Figure 12. Panel with installed test fixtures.

Prior to installing the panel in the test fixtures, a rectangular assembly frame was fabricated using lightweight metal C-channel stock. The vertical fixtures were placed on the assembly frame, adjusted until they were square and parallel, and then temporarily attached to the assembly frame with C-clamps. Both the panel vertical edges and vertical fixture contact surfaces were first covered with a layer of Teflon tape to minimize friction. The panel was then installed in and aligned with the vertical fixtures, as shown in Figure 11. The green assembly frame and C-clamp are also evident in the figure.

The eleven Allen-head studs on each vertical fixture were gradually tightened to force the two half-cylindrical steel contact surfaces closer together and into contact with the panel front and back surfaces. Because of the raised tow overlaps, the vertical fixture and back of the panel are not in continuous contact, but rather touch at seven discrete points per edge. Once the panel edge was completely straightened,

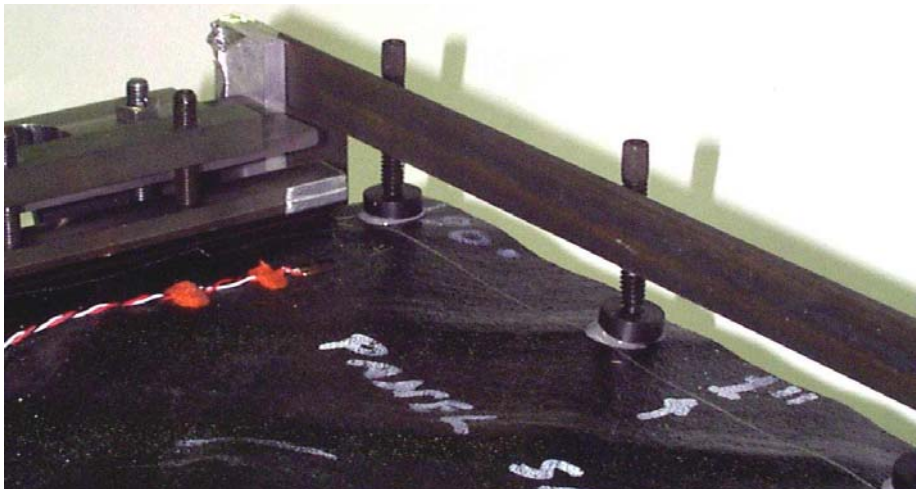

Figure 13. Detail of panel with installed test fixtures.

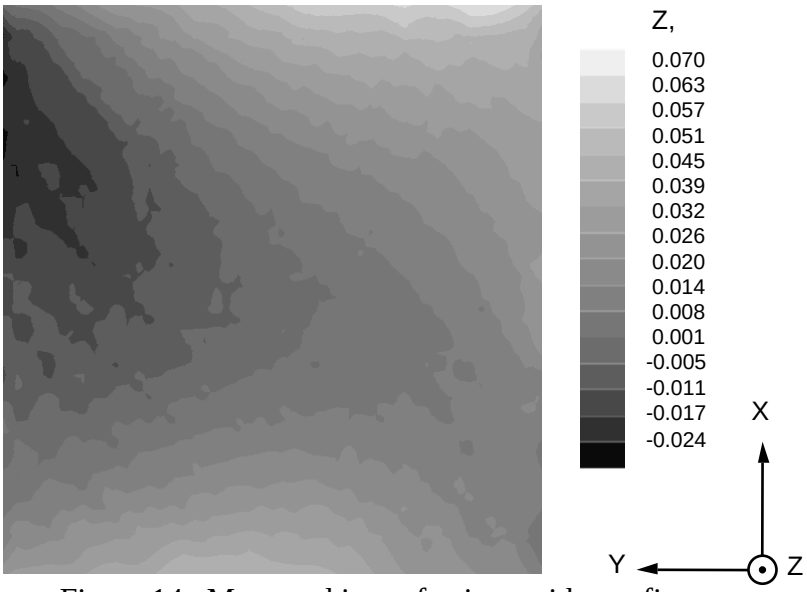

Figure 14. Measured imperfections with test fixtures.

the studs were all set to the same torque using a torque wrench to ensure a uniform clamping force along the vertical edges, and then fixed in place with epoxy. Great care was also taken to not overtighten the studs, as this would have damaged the panel surface.

The front set of swivel pads on the horizontal fixtures were first aligned level and fixed in place using epoxy, since they would be in contact with the smooth front surface of the panel. A 1/4 inch-thick spacer plate was placed between the ends of the vertical fixtures and the horizontal fixture, and held in lightly place with nuts and threaded rods. These spacer plates ensured that there was 1/2-inch of axial displacement available under axial loading. The horizontal fixture was adjusted transversely to align it with the panel axial centerline. The back set of swivel pads on the horizontal fixtures were then tightened to flatten the horizontal edge of the panel, set with a torque wrench, and fixed in place with epoxy. The panel with all of the vertical and horizontal edge test fixtures installed is shown in Figure 12, with a detail view of one corner of the panel shown in Figure 13.

The spacer plates were then removed, and L-shaped steel fittings were attached with bolts at each corner of the horizontal fixtures. These eight fittings ensured that the vertical fixtures could only move axially and normal to the panel horizontal fixtures. The panel was then reoriented and supported vertically, and epoxy potting was cast into the horizontal fixtures to a depth of 1 inch. After the potting had completely hardened, the potting and encapsulated panel horizontal edges were ground flat and parallel using an end mill.

The coordinate measuring machine was then used to resurvey the panel to determine its geometric imperfections with the attached test fixtures. The measured front surface imperfections taken within the 24 inch-square test section were then input as applied normal displacements to a finite element model of the flat plate to estimate the panel displacements within the test fixtures and at other locations obscured by strain gages and wiring. This combined set of measured and estimated geometric imperfections is shown in Figure 14, and demonstrate that application of

the test fixtures greatly reduced the geometric imperfections in the panel from the case without test fixtures discussed earlier. The maximum deflection for the panel with test fixtures was 0.070 inches and the minimum value was –0.024 inches, while the root-mean-square deflection was reduced by nearly a factor of eight to 0.023 inches, or about 13 percent of the average panel thickness.

PANEL END COMPRESSION TEST

The panel and its attached test fixtures were then installed in a 300 klb-capacity mechanical test stand for the end compression test. The front and back of the panel in the test stand are shown in Figures 15a and 15b. The photograph of the panel front also shows part of the shadow moiré system used for qualitative measurement of the panel normal deflections. Affixed to a clear Lexan sheet mounted in front of the panel, this grid is comprised of a set of thin, equally spaced black lines used to project shadows from a polarized light onto the white-painted front of the panel.

Instrumentation for the panel test included four linear variable differential transformers (LVDTs) located at the corners of the test stand to measure the panel end shortening, and one LVDT at the panel center to measure the panel out-of-plane deflection. Two additional LVDTs were also used to measure the relative Z-displacement and axial rotation of the test stand platens. Twenty-eight strain gages, arranged in front-and-back pairs, were deployed along the panel axial and transverse centerlines. Three additional pairs of strain gages were located along the upper edge of the panel to facilitate pretest load balancing. The applied axial load was measured using a load cell permanently mounted on the test stand.

Figure 15a. Front of panel test setup.

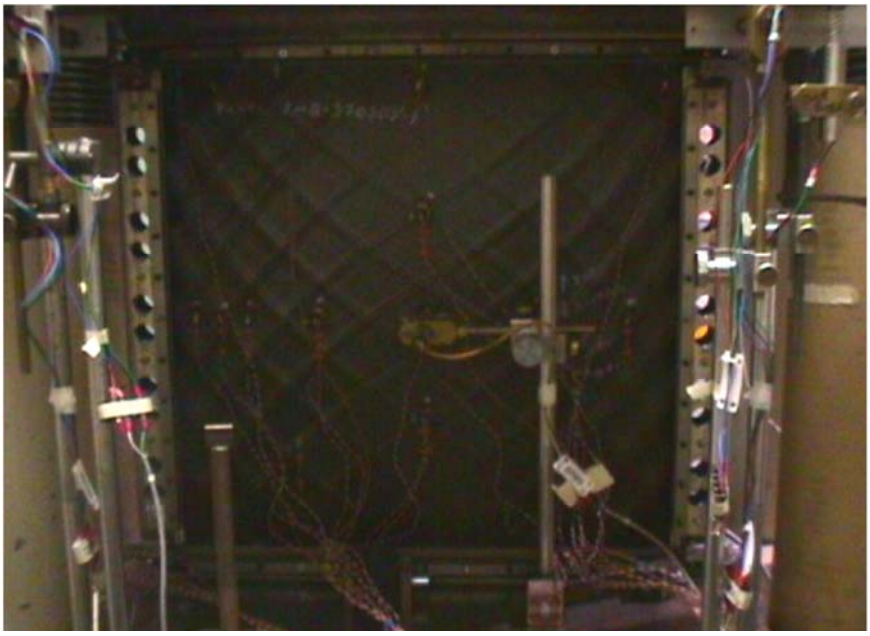

Figure 15b. Back of panel test setup.

The panel was then loaded to failure in a displacement-control mode at a load rate of approximately 2 klb/min. The average axial deflection of the panel was computed from the four LVDT readings at the platen corners, and is plotted against the corresponding axial load in Figure 16. The average axial deflection shown has been shifted to permit the panel linear prebuckling response to pass through the plot origin. The best-fit slope of the linear prebuckling response is defined as the

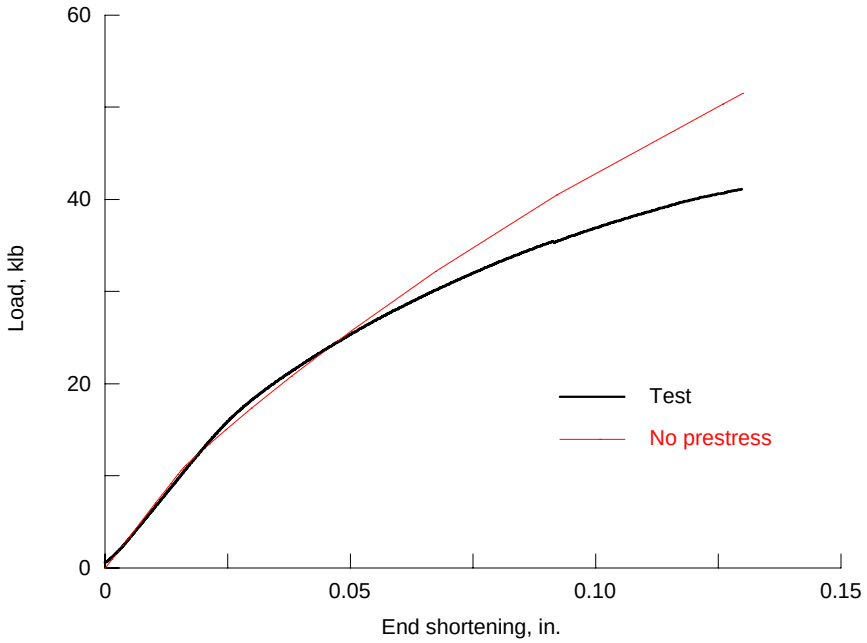

Figure 16. Load vs. axial deflection.

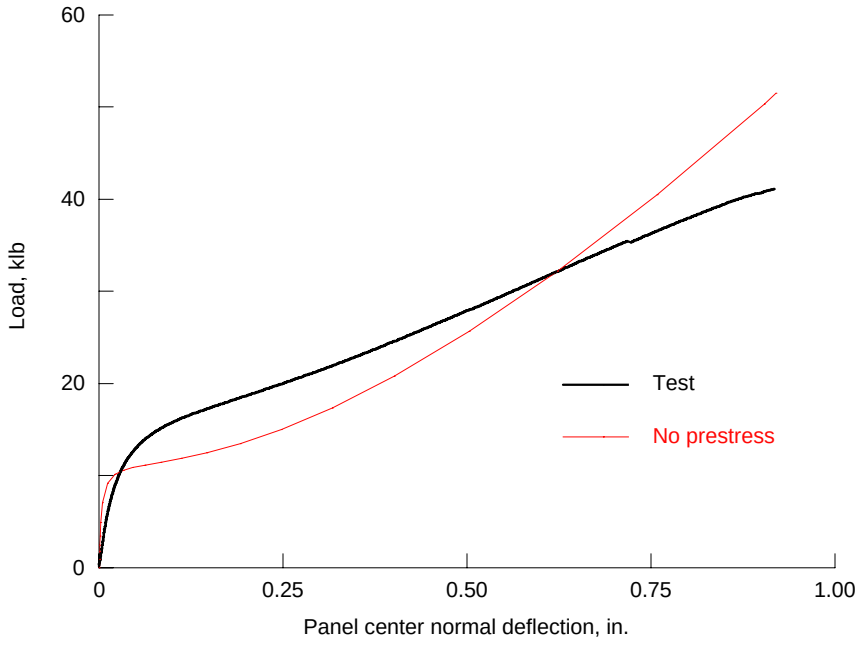

Figure 17. Load vs. normal deflection.

panel axial stiffness, and is computed as 649.86 klb/in. between 2 and 13 klb applied load. Above 13.6 klb load, the axial deflection became increasingly nonlinear and the axial stiffness decreased until the panel finally failed at 41.1 klb applied load. The average measured axial deflection at failure was 0.130 inches.

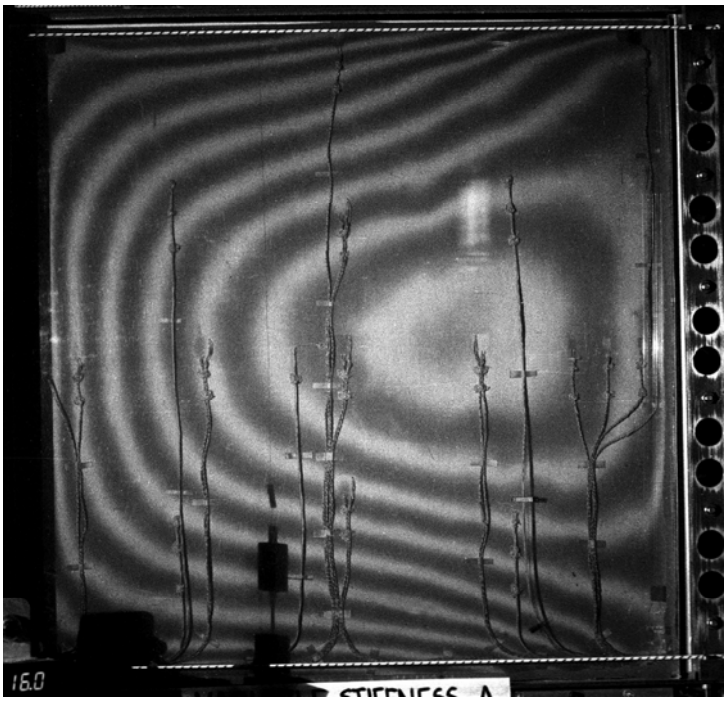

Figure 18a. Observed normal deflections at 16 klb.

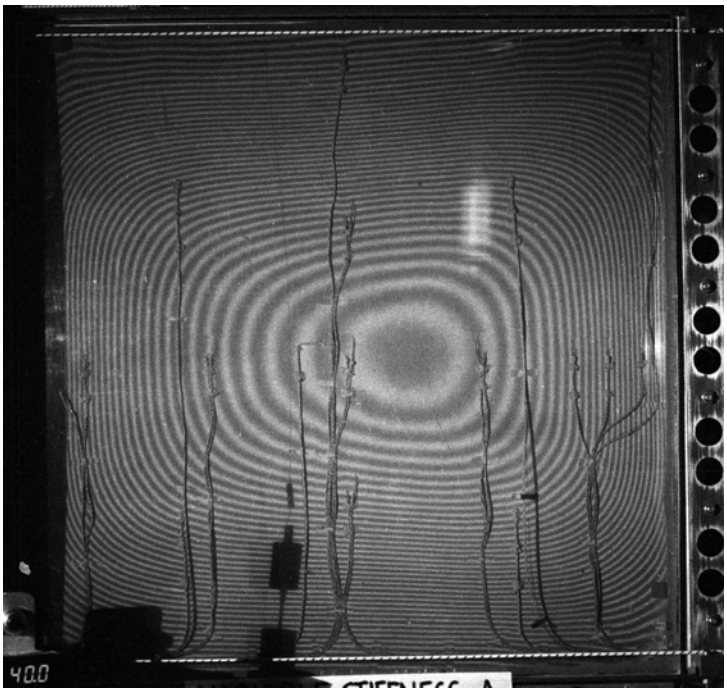

Figure 18b. Observed normal deflections at 40 klb.

The measured normal deflection at the panel center is plotted in Figure 17. The deflection increased slowly below about 18 klb, and then increased in a roughly linear manner to 0.917 inches at failure. Small discontinuities were observed in the measured load-deflection curves of Figures 16 and 17, which were indicative of a local failure somewhere within the panel near 35 klb load. Shadow moiré

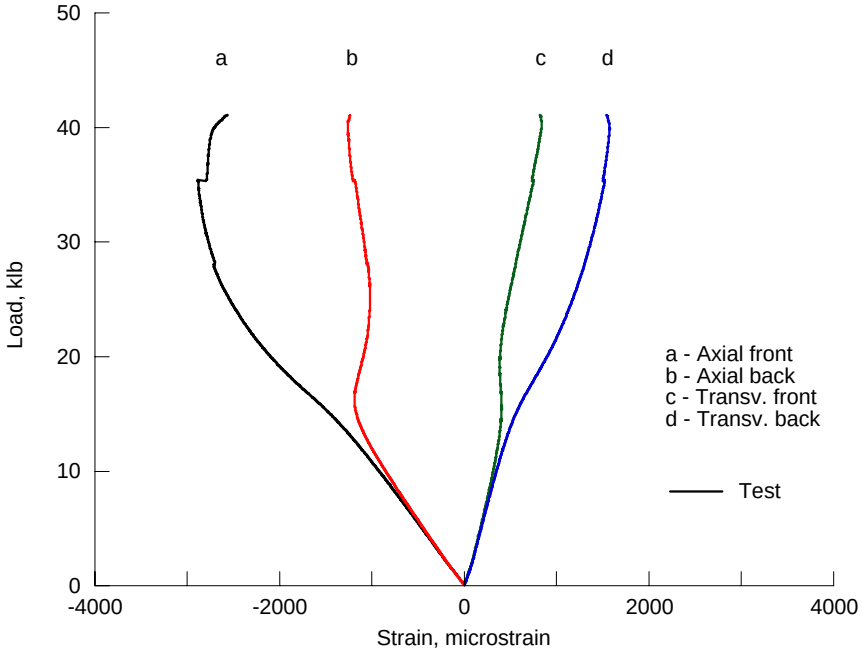

Figure 19. Load vs. strain at panel center.

photographs of the panel normal deflections at 16 and 40 klb are shown in Figures 18a and 18b, respectively. The larger number of contours in the latter figure corresponds to the higher normal deflections at the higher load. In this figure, the locations of the maximum measured deflections appeared to be offset from the panel center. However, further examination of the strain data indicated that this offset was actually due to the polarized light source location.

Axial and transverse strains from gages located at the panel center are also plotted against the axial load in Figure 19. The strains are very close at low loads and diverge slowly up to about 16 klb load, which indicates that minimal bending is taking place. At loads above 16 klb, the back-to-back strains diverge rapidly, and bending at the panel center increases as the response moves deeper into the postbuckling region. Using the test data plotted in these figures, the panel experimental buckling load is estimated to be 17.5 klb, with a coefficient of variation of 8.6 percent.

PRELIMINARY END COMPRESSION ANALYSIS

Bifurcation buckling and geometrically nonlinear analyses were first performed using the panel finite element model shown in Figures 5 to 7. Boundary conditions for this analysis were clamped loaded edges with a specified axial deflection on the panel upper edge, w = 0 within the potted ends, and w and Ry = 0 along the simply supported vertical edges. Measured geometric imperfections for the panel with test fixtures (see Figure 14) were used as initial imperfections in this analysis without prestresses. The predicted buckling load from this analysis was 11.6 klb, which was much lower than the measured buckling load of 17.5 klb.

A geometrically nonlinear analysis of this case was then performed with an applied end shortening of 0.130 inches. The predicted load and deflections from this analysis are plotted in Figures 16 and 17 with the corresponding test data. While close during linear prebuckling, the analytical axial deflections were

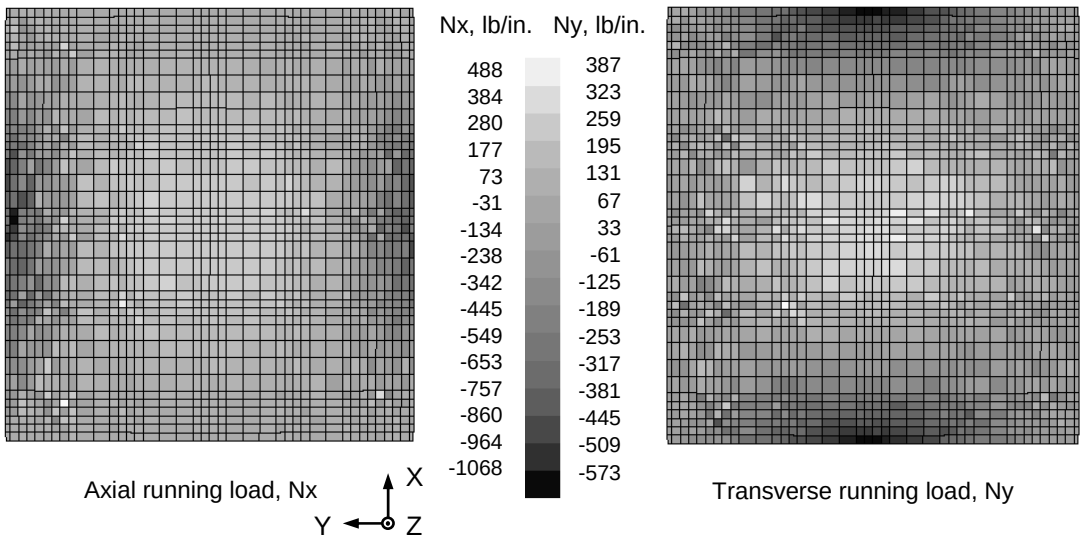

Figure 20. Internal running loads from mechanical prestress.

overpredicted near buckling, and then underpredicted at higher load levels. This trend was replicated for the normal deflections, although the differences observed between predicted and measured results were more exaggerated than for the axial deflections. Therefore, these results clearly demonstrated that this analysis with only geometric imperfections was not sufficient to predict the actual structural response of the panel.

MECHANICAL PRESTRESS ANALYSIS

To better correlate the test and analysis results for the composite panel, the measured panel imperfections in Figures 8 and 14 were used to generate a set of mechanical prestresses. This internal stress state was intended to replicate the actual prestresses imposed on the panel during installation of the test fixtures. This analysis implicitly assumed that the panel with imperfections was in a stress-free state after curing.

The geometric imperfections measured after installation of the test fixtures (Figure 14) were subtracted from the measured geometric imperfections taken after completion of the panel curing process (Figure 8). This full-field set of deformations was then imposed as applied displacements onto the finite element model of the cured panel, thus forcing the model into the fixtured configuration. Predicted internal stress resultants Nx and Ny generated in the panel are shown in Figure 20. The panel center has large tensile loads in both directions, with compressive stresses along the free edges parallel to the axes of the running loads.

REFINED END COMPRESSION ANALYSIS AND TEST CORRELATION

The mechanical prestresses described above were then incorporated into finite element analyses of the panel end shortening. After application of the displacements required to force the panel into its fixtured configuration, the structural test boundary conditions described previously were then applied. An analysis that included geometric nonlinearities was performed with a maximum applied end shortening of 0.130 inches.

Predicted axial and normal deflections from this analysis are plotted in Figures 21 and 22, respectively, along with the corresponding measured data. These results show much better correlation than the previous analyses without prestresses, and agree throughout prebuckling and into the postbuckling region. However, the correlation between analysis and experiment begins to break down in the mid-postbuckling range, and diverges rapidly as the panel approaches failure.

To determine if this poor correlation at higher loads was due to material effects, a nonlinear material model [9] was used. This composite ply model, included as an option in the STAGS code, treated the fiber and transverse responses linearly, and used a nonlinear cubic polynomial to model the shear strain-stress relationship. The coefficient S_{6666}, varied over a range of integer values, was used to control the degree of material nonlinearity in the model. Parametric analyses with both geometric and increasing material nonlinearity were then performed for the panel.

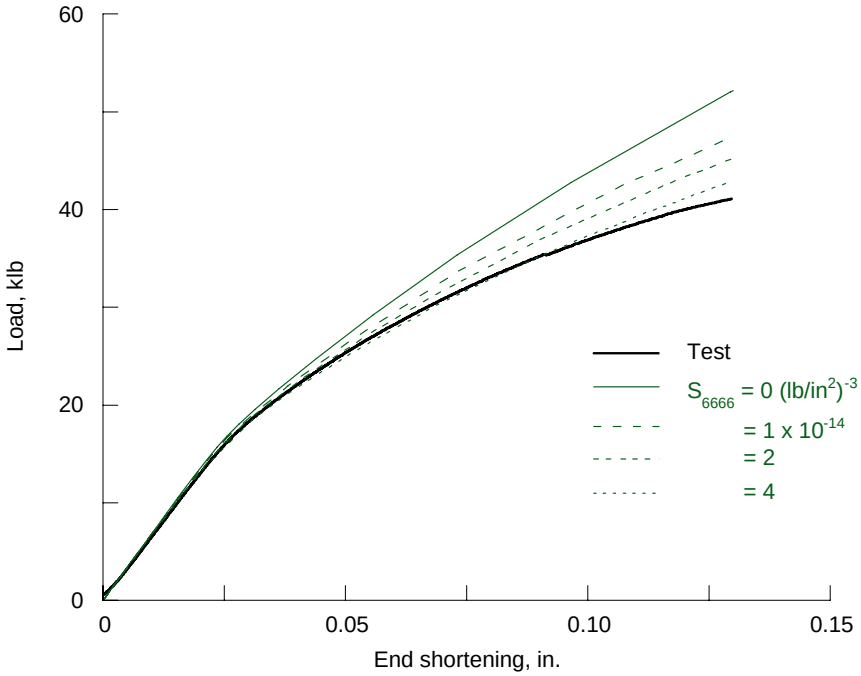

Figure 21. Load vs. axial deflection.

The results of these analyses are plotted in Figure 21 for comparison with the test data. The analysis with $S_{6666} = 0$ was identical to an analysis with a linear material response evaluated earlier. Qualitatively, the best correlation between the test data and the analysis with both geometric and material nonlinearities is observed for $S_{6666} = 4 \times 10^{-14}$ $(lb/in2)^{-3}$. Analysis results for this value of S_{6666}

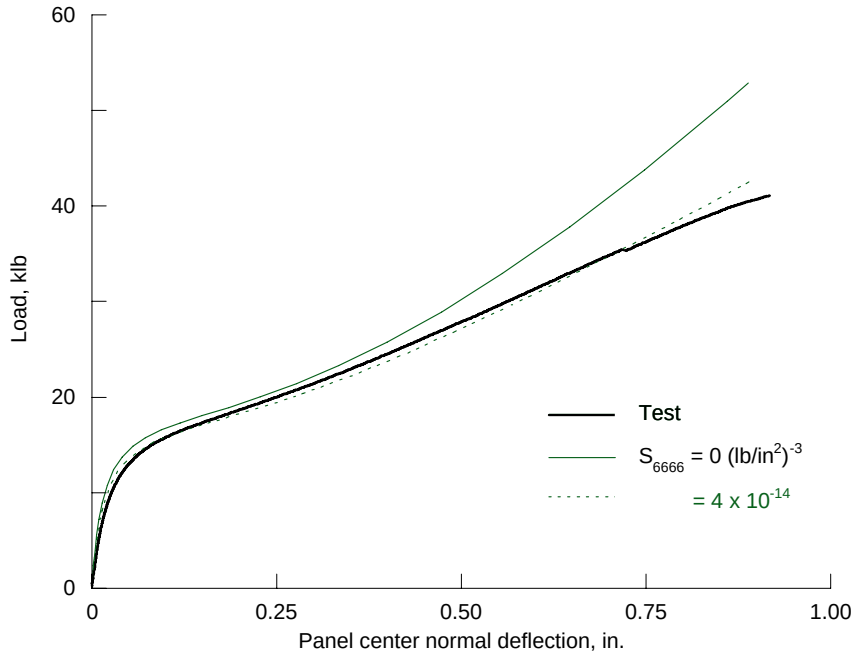

Figure 22. Load vs. normal deflection.

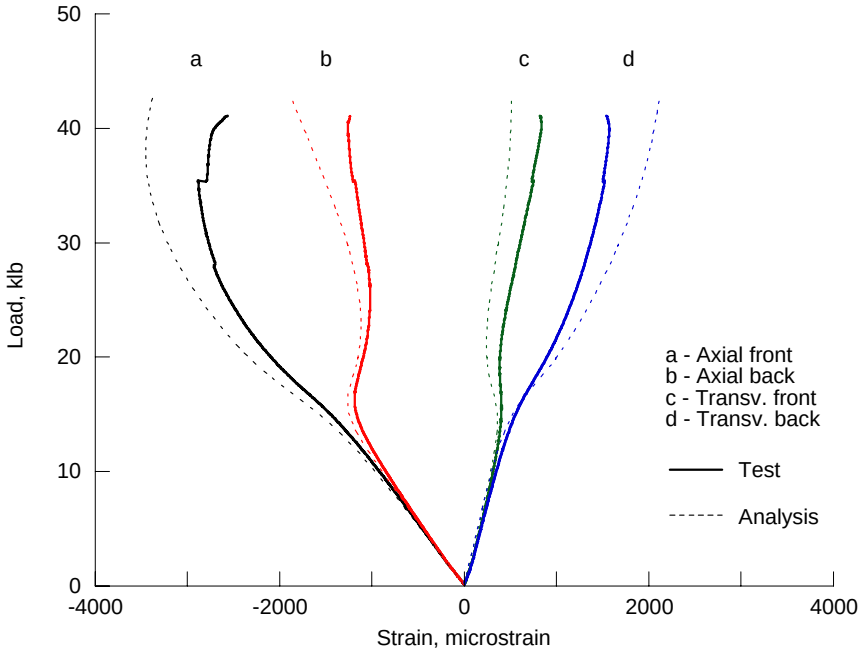

Figure 23. Load vs. strain at panel center.

are plotted in Figures 22 and 23 for the normal deflection and strains (respectively) at the panel center, and also agree well with the corresponding experimental results.

Predicted panel normal deflection contours at the maximum axial displacement of 0.130 inches are shown in Figure 24. The predicted axial load at this end shortening is 42.9 klb, with a predicted panel center normal deflection of 0.891 inches. The corresponding measured results at the same end shortening are 41.1 klb axial load and an 0.917-inch deflection at the panel center, which are both very close to the analytical predictions.

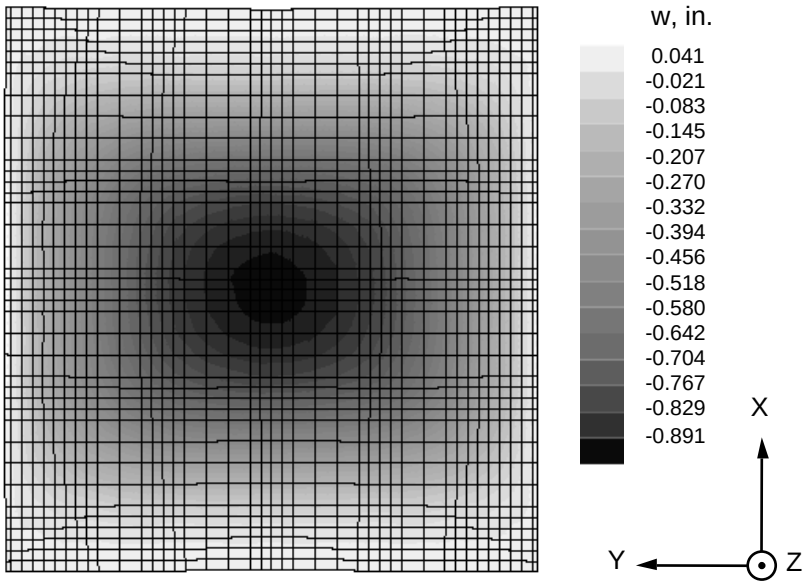

Figure 24. Predicted normal deflections at u = 0.130 inches.

CONCLUDING REMARKS

The structural response of a tow-steered composite panel was evaluated using both experimental and finite element methods. The panel test required the development of special test fixtures to greatly reduce the large geometric imperfections present in the cured panel. Under end compression loads, the panel exhibited a linear prebuckling response, which was followed by a transition to a nonlinear postbuckling state.

The panel finite element model captured variations in laminate thicknesses and fiber angles present in the hardware. A geometrically nonlinear analysis under a postcure thermal load replicated the geometric imperfections measured at room temperature. However, a geometrically nonlinear analysis with measured imperfections for the panel mounted in the test fixtures predicted the correct prebuckling stiffness, but underpredicted the panel buckling load.

Measured imperfections for the panel (both without and with the test fixtures) were then used to model the internal prestresses resulting from installation of the panel in the test fixtures. When these prestresses were included in the end compression analysis, the predicted response was much closer to the measured data up through panel buckling and into postbuckling. However, the test and analysis data still gradually diverged with increasing load. Inclusion of material nonlinearity effects resulted in much closer correlation up to the panel failure load.

The analyses and tests described herein show that determining the structural response of a composite panel with large geometric imperfections can be very complicated. These methods were successfully implemented to characterize the response of this tow-steered, variable stiffness panel from linear prebuckling through nonlinear postbuckling, and up to global failure.

REFERENCES

1. Dano, M.-L. and M. W. Hyer. 1998. "Thermally-Induced Deformation Behavior of Unsymmetric Laminates," *International Journal of Solids and Structures*, 35(17):2101-2120.
2. Schlecht, M., K. Schulte and M. W. Hyer. 1995. "Advanced Calculation of the Room-Temperature Shapes of Thin Unsymmetric Composite Laminates," *Composite Structures*, 32:627-633.
3. Hilburger, M. W., M. P. Nemeth, J. C. Riddick and R. P. Thornburgh. 2004. "Effects of Elastic Edge Restraints and Initial Prestress on the Buckling Response of Compression-Loaded Composite Panels," presented at the 45th AIAA/ASME/ASCE/AHS/ASC Structures, Structural Dynamics and Materials Conference, April 2004.
4. Thornburgh, R. P. and M. W. Hilburger. October 2005. "Identifying and Characterizing Discrepancies Between Test and Analysis Results of Compression-Loaded Panels," NASA/TM-2005-213932 or ARL-TR-3664.
5. Tatting, B. F. and Z. Gürdal. 1998. "Design and Manufacture of Tow-Placed Variable Stiffness Composite Laminates with Manufacturing Considerations," presented at the 13th U.S. National Congress of Applied Mechanics, June 1998.
6. Evans, D. O., M. M. Vaniglia and P. C. Hopkins. 1989. "Fiber Placement Process Study," presented at the 34th International SAMPE Symposium, May 1989.
7. Gürdal, Z. and R. Olmedo. 1993. "In-Plane Response of Laminates with Spatially Varying Fiber Orientations: Variable Stiffness Concept," *AIAA Journal*, 31(4):751-758.

8. Rankin, C. C., F. A. Brogan, W. A. Loden and H. D. Cabiness. 2005. *STAGS User Manual, Version 5.0*, LMSC P032594, Lockheed Martin Missiles & Space Co., Inc., Palo Alto, California.
9. Hahn, H. T. and S. W. Tsai, 1973. "Nonlinear Elastic Behavior of Unidirectional Composite Laminae," *Journal of Composite Materials*, 7(1):102-118.